IEEE Access
Multidisciplinary ⋮ Rapid Review ⋮ Open Access Journal

Received May 10, 2020, accepted June 5, 2020, date of publication June 9, 2020, date of current version June 18, 2020.

Digital Object Identifier 10.1109/ACCESS.2020.3001076

Dynamic Analysis and Model Order Reduction of Virtual Synchronous Machine Based Microgrid

WENQIANG HU[1], (Student Member, IEEE), ZAIJUN WU[1], (Member, IEEE), AND VENKATA DINAVAHI[2], (Fellow, IEEE)

[1]School of Electrical Engineering, Southeast University, Nanjing 210096, China
[2]Department of Electrical and Computer Engineering, University of Alberta, Edmonton, AB T6G 2V4, Canada

Corresponding author: Zaijun Wu (zjwu@seu.edu.cn)

This work was supported in part by the National Natural Science Foundation of China under Grant 51977034, in part by the National Key Research and Development Program of China under Grant 2016YFB0900504, and in part by the Natural Science and Engineering Research Council of Canada (NSERC). The work of Wenqiang Hu was supported by the China Scholarship Council (CSC).

ABSTRACT The concept of virtual synchronous machine (VSM) was proposed to deal with the shortcomings of low inertia and damping of traditional control strategies for power electronic converters. But what if all distributed energy resources and controllable loads in a microgrid adopt the VSM control strategy, and will it present better performance than conventional droop control-based microgrid (DMG)? In this paper, the VSM-based microgrid (VSMG) is analyzed. The small-signal modeling of the VSMG is studied at first. Then static stability and dynamic characteristics of the VSMG are analyzed and compared with the DMG in both frequency-domain and time-domain. With the growing scale of microgrids, their modeling and simulation are becoming significant computational burdens. Inspired by the participation factor analysis of the VSMG and the concept of coherency in power systems, the VSMG small-signal model is equivalent to a modified third-order synchronous generator (SG) model in this paper. The equivalencing involves gray-box system identification and is realized by estimating equivalent electrical parameters alternately and iteratively. The equivalent SG (EqSG) model is compared with three representative model order reduction methods to verify its effectiveness. Simulation results confirm the accuracy of the EqSG model substituting detailed VSMG model in time-domain simulations.

INDEX TERMS Microgrid modeling, model order reduction, virtual synchronous machine, small-signal modeling.

I. INTRODUCTION

With high penetration of distributed energy resources (DERs) and mass access of controllable loads, power systems are experiencing a paradigm shift from centralized and rotational generator-dominated systems to distributed and inverter-dominated systems [1]. In the modern power system, DERs and controllable loads are often integrated into a microgrid, and the hierarchical structure of microgrid - microgrid groups - active distribution network (ADN) is constructed. Microgrids not only promote the integration of renewable resources, but also improve the control flexibility of power systems [2]. However, the extensive introduction of power electronic devices reduces the overall inertia level and damages the frequency stability of power systems [3], which is more prominent in microgrids. This is because conventional control strategies for grid-connected inverters, such as PQ control and droop control strategies, lack inertia and damping as synchronous generators (SGs). To deal with this dilemma, the technology of virtual synchronous machine (VSM) [4] was proposed to provide inertia support to power systems. Although control strategies emulating virtual inertia in existing literatures, such as VSM [5], virtual synchronous generator [6], [7], synchronverter [8] and demand side VSM [9], were slightly different from each other, the principles were similar in the aspect that all of them mimic the inertial characteristic of the SG by emulating its fundamental swing equation. Thus, it is widely recognized that control strategies providing virtual inertia by introducing the swing equation can be classified as VSM control.

But whether the introduction of VSM technology into microgrids will improve their dynamic responses and static stabilities still requires research and verification. VSM control was compared with frequency droop control in [10], and

The associate editor coordinating the review of this manuscript and approving it for publication was Junjian Qi.

it concluded that both schemes could be regarded as equivalence under certain conditions. But the low-pass filter (LPF) of the measured output power was ignored in the VSM control scheme, which was not in accord with the practical application. Besides, only the frequency-active power (f-P) response was analyzed and the coupling interaction between voltage and active power was dismissed, i.e., a low R/X ratio was considered as an implicit assumption, which was not suitable for the microgrid practice. Comparisons of dynamic characteristics between VSM control and droop control was discussed in [11], and it demonstrated that VSM control had better frequency stability than droop control. It was proved in [12] that frequency resonance between SGs could be suppressed with the introduction of a VSM. However, only single-VSM scenario and SG-connected scenario were considered in [11] and [12], which was too simple to meet the scale of an actual microgrid. Besides, few researches considered the demand side VSM in a microgrid.

To analyze dynamic characteristics of a microgrid, the first step is its small-signal modeling [13]. A practical microgrid can be described by numerous nonlinear differential algebraic equations (DAEs). The small-signal model is obtained by linearizing the nonlinear DAEs around a set of steady-state operating points. However, for microgrids, their small-signal models exhibit multi-time scale characteristics, which requires small time steps for fast dynamics and a long simulation time to capture slow dynamics [14]. With the growing scale of microgrids, their time-domain simulations are becoming time-consuming and computational burdens. The necessity of model order reduction (MOR) for microgrids has never been more obvious.

According to [15], MOR methods are generally classified into three categories, i.e., polynomial approximations, state truncations and parameter optimizations. Polynomial approximation methods are based on matching moments or Markov parameters between the original and reduced-order models, which are applied to transfer function models, e.g., Padé approximation (PA). State truncation methods usually involve transformations of the original state-space model to reconfigure states according to observability, controllability or response time, etc., and elimination of ''less significant'' states, e.g., balanced transformation (BT) method and singular perturbation (SP) method. Parameter optimization approaches are based on optimizing parameters of reduced-order models to minimize errors of response data between reduced and original models, e.g., gray-box system identification.

As small-signal models of microgrids are often described in state-space forms, polynomial approximation methods were seldom used in microgrids MOR, whereas state truncation methods, especially the SP method, were commonly used methods. In [16], the SP method was used to obtain reduced-order models for islanded microgrids by exploiting different dominant time constants. Stability properties of the reduced model turned out to be consistent with the original model, so that the stability analysis of islanded microgrids could be simplified. In [17], the SP method was used to obtain the reduced-order small-signal model of a microgrid in both grid-connected and islanded conditions. Time-domain dynamic responses of the reduced model presented slight difference against the full-order model. In [18], the SP method and Kron reduction were combined to reduce large-signal dynamic models of islanded microgrids in temporal and spatial aspects, respectively. In [19], a method properly eliminating fast states of network dynamics was proposed for microgrids to predict stable regions of droop coefficients more accurately than the quasi-stationary reduced model neglecting all network dynamics. However, the common disadvantage of these methods is that the states in reduced-order models lose their original physical meanings.

The parameter optimization approach can also be interpreted as developing the dynamic equivalent model. In [20], the evolutionary particle swarm optimization based gray-box system identification was used to obtain an equivalent model for f-P dynamics of a microgrid. In [21], [22], black-box models for microgrids using the Prony method were proposed based on measurements of voltage, current and output power at the point of common coupling (PCC). In [23], a novel structure gray-box model including basic electrical components was proposed for microgrid system identification. The identification procedure was carried out by four genetic algorithm-based optimization steps using measurement data at the PCC. The common disadvantage of these methods is that the accuracy of reduced models is affected by the scale of measurement data.

In this paper, the VSM-based microgrid (VSMG) is studied, in which both DERs (including energy storage systems) and controllable loads (with rectifiers at their front end) all adopt VSM control. In the frequency-domain, modal analysis is applied to the VSMG small-signal model to clarify the interaction between states and modes in the VSMG. Besides, bode plots, eigenvalue trajectories and time-domain dynamic responses of various scenarios are comparatively analyzed between VSMG and droop control-based microgrid (DMG) to figure out the influences of VSM control on dynamic characteristics of microgrids. Inspired by the conclusion of participation factor analysis and the thought of coherency in power systems, a new MOR method for VSMG is proposed by equivalencing the detailed small-signal model to a modified third-order SG model. The proposed equivalent SG (EqSG) method derives equivalent electrical parameters for the VSMG and remains certain physical meanings in the reduced states without relying on measurement data.

The remainder of this paper is organized as follows. The detailed small-signal model of the VSMG is built in Section II. Static stability and dynamic characteristics of the VSMG are analyzed and compared with the DMG in Section III. Then in Section IV, three representative MOR methods, i.e., BT, SP and poles clustering-based PA (PCPA) methods, are reviewed and applied to the VSMG model. In Section V, the proposed EqSG method is developed and introduced in detail. In Section VI, four MOR methods

are compared to summarize their advantages and disadvantages, and the effectiveness of the proposed method is verified through simulation studies. Finally, the conclusions are drawn in Section VII.

II. SMALL-SIGNAL MODELING OF THE VSMG

In this Section, modeling of the VSMG is analyzed and expressed in terms of DAEs at first. These equations are nonlinear and need to be linearized around a set of equilibrium points, i.e., small-signal modeling, to study the system static stability and dynamic responses. Structure of the studied VSMG is shown as Fig. 1, where DER1 (SG) at Bus0, DER2 (VSM) at Bus1 and a controllable load (VSM) at Bus2 are connected to a local load at Bus3 through three distribution lines. This microgrid is connected to the upstream network from Bus3 through a grid-connection line. In view of existing researches on DMG modeling [13], [18] and [24], this Section focuses on the distinctions appeared in VSMG modeling.

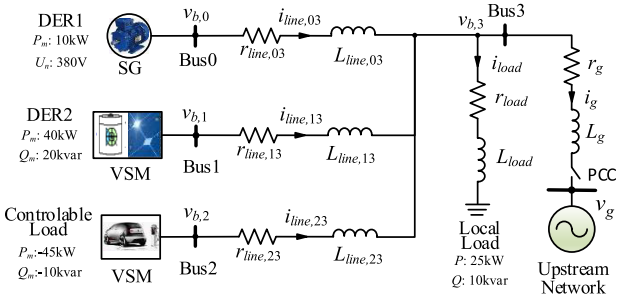

FIGURE 1. Structure of the studied VSMG.

A. MODELING OF A VSM

The block diagram of a VSM is shown in Fig. 2. The power part consists of a three-leg converter and a LC filter. Since the dc side of a VSM often contains an energy storage module to provide inertial energy support and responds fast enough to maintain dc voltage stable, it can be equivalent to an ideal dc source. The control part can be divided into three parts, i.e., VSM control loop, virtual impedance control and voltage current dual-loop control. The VSM model is implemented in its local rotational reference frame (dq-axis). Subscript d or q appeared in the following voltages and currents represents corresponding d or q axis component.

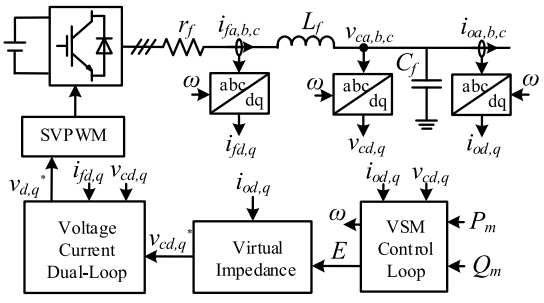

FIGURE 2. Block diagram of a VSM.

1) VSM CONTROL LOOP

VSM control loop generates the virtual internal electromotive force. The function of this loop is to control the output power of the converter. Active power control is realized by mimicking the swing equation:

$$J\dot{\omega} = (P_m - P_e)/\omega - D_p(\omega - \omega_n) \tag{1}$$

where J and D_p are virtual moment of inertia and virtual damping factor, respectively; ω_n and ω are nominal angular frequency and VSM's virtual angular frequency, respectively; P_m and P_e are active power reference and output active power, respectively. The dq-axis output voltage (v_{cd}, v_{cq}) and current (i_{od}, i_{oq}) measurements are used to calculate the instantaneous output active power, and a first-order LPF with the corner frequency ω_c is used to obtain P_e:

$$\dot{P}_e = 1.5\omega_c(v_{cd}i_{od} + v_{cq}i_{oq}) - \omega_c P_e \tag{2}$$

Note that the filtered output power is selected as the feedback power value, so as to attenuate potential ripples in the instantaneous power, which will reflect in frequency and magnitude of the voltage reference [7].

Its reactive power control mainly consists of a droop link and an integral link, so as to mimic voltage-reactive power (V-Q) droop characteristic and excitation inertia.

$$K\dot{E} = Q_m - Q_e - D_q(U - U_n) \tag{3}$$

where E is magnitude of the virtual internal electromotive force, $U = \sqrt{{v_{cd}}^2 + {v_{cq}}^2}$ is the output voltage magnitude, U_n denotes the nominal voltage magnitude, K and D_q are virtual excitation inertia factor and V-Q damping factor, respectively; Q_m and Q_e are reactive power reference and output reactive power, respectively. Similar to P_e, Q_e is the filtered instantaneous reactive power:

$$\dot{Q}_e = 1.5\omega_c(v_{cq}i_{od} - v_{cd}i_{oq}) - \omega_c Q_e \tag{4}$$

2) VIRTUAL IMPEDANCE CONTROL

Virtual impedance control generates the virtual stator terminal voltage reference ($v_{cd}{}^*$, $v_{cq}{}^*$). Its function is to simulate the stator impedance. It increases the output impedance to help inhibit harmonic circulation between paralleled VSMs and help the decoupling of active and reactive power control.

$$\begin{cases} v_{cd}{}^* = E - r_v i_{od} + \omega L_v i_{oq} \\ v_{cq}{}^* = -r_v i_{oq} - \omega L_v i_{od} \end{cases} \tag{5}$$

where r_v and L_v are virtual resistance and virtual inductance, respectively. Dynamics of the virtual inductance are not considered to avoid instability or poorly damped oscillations caused by the introduction of current derivative [25].

3) VOLTAGE CURRENT DUAL-LOOP CONTROL AND THE POWER PART

Voltage current dual-loop control generates voltage command for the space vector pulse width modulation (SVPWM), in which PI controllers are adopted. Its function is to control v_{cd} and v_{cq} tracking v_{cd}^* and v_{cq}^* promptly and errorlessly. As the modeling of PI controllers, voltage source converters and LC filters is identical between VSMs and droop control-based inverters, equations of this part are listed in Appendix A.

B. COMPLETE MICROGRID MODEL

Network dynamics are generally neglected in small-signal modeling of conventional power systems. However, in the case of microgrids, network dynamics can greatly influence the slow states associated with inverter power controllers [19] and further influence the system stability under certain circumstances [13]. Here, dynamics of the network and the local load are considered, and corresponding DAEs are presented in Appendix A.

Modeling of the SG considers dynamics of the prime mover (p_m), excitation (v_f), rotor rotation (ω_r), stator (φ_d, φ_q), field (φ_{fd}) and damper (φ_{kd}, φ_{kq}) windings, which was discussed in detail in [26]. Then, combining all the DAEs of each component mentioned above, the nonlinear model of the studied VSMG can be established in the format as (6).

$$\begin{cases} \dot{x} = f(x, u) \\ y = g(x, u) \end{cases} \tag{6}$$

where y is the output vector, which is determined according to research needs, x and u denote the state vector and the input vector, respectively. For the islanded VSMG, $u = [\, r_{load} \; L_{load} \,]^T$, where r_{load} and L_{load} are resistance and inductance of the local load, respectively. And for the grid-connected VSMG, $u = [\, \omega_g \; U_g \,]^T$, where ω_g and U_g denote angular frequency and voltage magnitude of the upstream network at PCC, respectively.

C. SMALL-SIGNAL MODEL OF THE SYSTEM

The small-signal model is obtained by linearizing (6) at a set of equilibrium points. There are two ways of finding equilibrium points. One method is to set the left part of the differential equations in (6) to zero, as $0 = f(x, u)$, and then solve these equations to determine the equilibrium points. The other is to simulate the nonlinear model and take a snapshot at a certain time when the system reaches steady-state. Because both methods yield same results, the simulation-based method was used in this paper. System parameters of the studied VSMG are displayed in Appendix A. The small-signal model represented in the state-space format as (7) can be generated using MATLAB Symbolic Math Toolbox.

$$\begin{cases} \Delta\dot{x} = A\Delta x + B\Delta u \\ \Delta y = C\Delta x + D\Delta u \end{cases} \tag{7}$$

where Δ denotes small disturbance.

As the following dynamic analysis focuses on the influences introduced by VSM control in a microgrid and the comparison of dynamic characteristics between VSMG and DMG, only local control is considered in the microgrid modeling. Besides, the studied DMG maintains the same network structure and system parameters as the VSMG except for the power control loop. In the studied DMG, the power control loop of DER2 adopts the droop control strategy:

$$\omega = \omega_n + K_f(P_m - P_e) \tag{8}$$

$$E = U_n + K_v(Q_m - Q_e) \tag{9}$$

where droop coefficients K_f and K_v are determined by realizing the same steady-state droop effect as D_p and D_q, respectively, according to (10).

$$\begin{cases} K_f = 1/(\omega_n D_p) \\ K_v = 1/D_q \end{cases} \tag{10}$$

Besides, the controllable load in the VSMG is substituted by a constant load with the same power consuming in the DMG.

III. DYNAMIC ANALYSIS OF THE VSMG

A. FREQUENCY-DOMAIN ANALYSIS

Because the islanded operation of microgrids is more prone to instability, the frequency-domain analysis is mainly focused on the islanded VSMG. All eigenvalues (λ_{1-42}) of the islanded VSMG are listed in Appendix B and corresponding eigenvalue spectrum is shown in Fig. 3. As λ_{39-42} are far from the imaginary axis and have little influence on the stability and dynamics of the system, they are not shown in Fig. 3. The eigenvalue spectrum can be divided into three groups according to its distribution in the s plane. The eigenvalues in group 1 are close to the imaginary axis and are critical to the small-signal stability. It is necessary to analyze which states are sensitive to these eigenvalues.

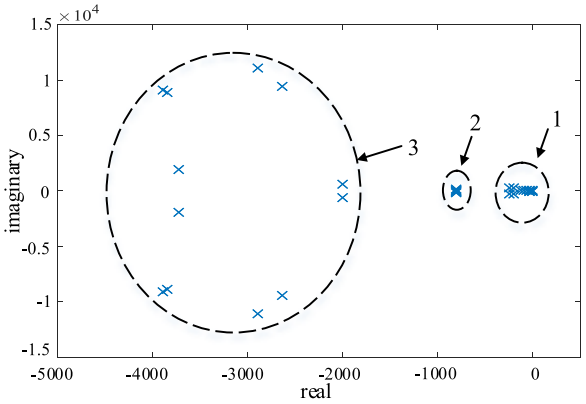

FIGURE 3. Eigenvalue spectrum of the studied VSMG.

1) PARTICIPATION FACTOR ANALYSIS

Participation factor reflects the degree of each state participating in every mode (eigenvalue). Assume w_i^T and v_i are

respectively the left and right eigenvectors corresponding to λ_i of matrix A. The components of v_i indicate the relative activity of each state in the ith mode. The components of ${w_i}^T$ weight the effect of initial conditions in exciting the ith mode. The normalized participation factor is defined as:

$$p_i = \frac{\left|{w_i}^T\right| |v_i|}{\sum_{k=1}^{N} \left(\left|{w_k}^T\right| |v_k|\right)} \tag{11}$$

where N is the number of eigenvalues.

Using (11), major participants of each mode can be found, which are listed in Appendix B. Eigenvalues in group 3 are mainly influenced by the states derived from the local load, LC filters and the network impedance. Eigenvalues $\lambda_{29-32,35-38}$ have relatively high natural frequency, which is determined by the inherent resonance characteristic of LC filters. Eigenvalues $\lambda_{33,34}$ indicate that dynamics of the network should not be ignored in the microgrid modeling, because this pair of conjugate eigenvalues is mainly stimulated by the interaction of LC filters and the network impedance. In terms of eigenvalues in group 2, they are mainly affected by the current controllers of VSMs and the stator inductance of the SG. Eigenvalues λ_{21-24} indicate that PI parameters in the current controllers are well-designed as these modes are well-damped and have relatively small time constants. As for eigenvalues in group 1, the states that have relatively large participation factors are mainly from the SG and VSM control loop. Thus, these states are crucial in influencing the small-signal stability. Furthermore, eigenvalues in group 1 have relatively large time constants, which indicates that they are slow dynamics in the transient process. In other words, the quality of dynamic responses is mainly influenced by the states derived from the SG and VSM control loop.

2) FREQUENCY RESPONSE COMPARISON

Fig. 4 compares bode plots of islanded VSMG and DMG. It can be seen form Fig. 4(a) and (b) that the difference of frequency characteristics only occurs in the low frequency band. Besides, the absolute amplitude gain is smaller in the case of VSMG than that of DMG, which indicates the voltage frequency and magnitude of VSMG are less disturbed when the local load changes.

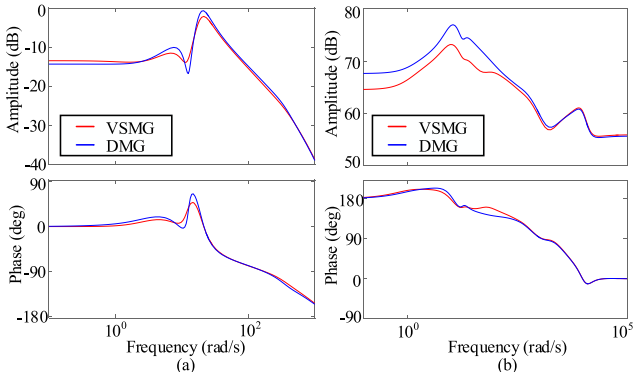

FIGURE 4. Bode plots of islanded VSMG and DMG: (a) frequency-domain response from Δr_{load} to voltage frequency of Bus3, (b) frequency-domain response from ΔL_{load} to voltage magnitude of Bus3.

3) SMALL-SIGNAL STABILITY COMPARISON

In order to test small-signal stabilities of islanded VSMG and DMG, trajectories of dominant eigenvalues are derived by varying the local load, damping factors (droop coefficients) and virtual impedance parameters in the small-signal models, as shown in Fig. 5, where arrows specify increasing of corresponding parameters. The influence of changing virtual inertia parameters is not analyzed here as it was discussed in [6] and [11] and cannot form a comparative analysis with the DMG.

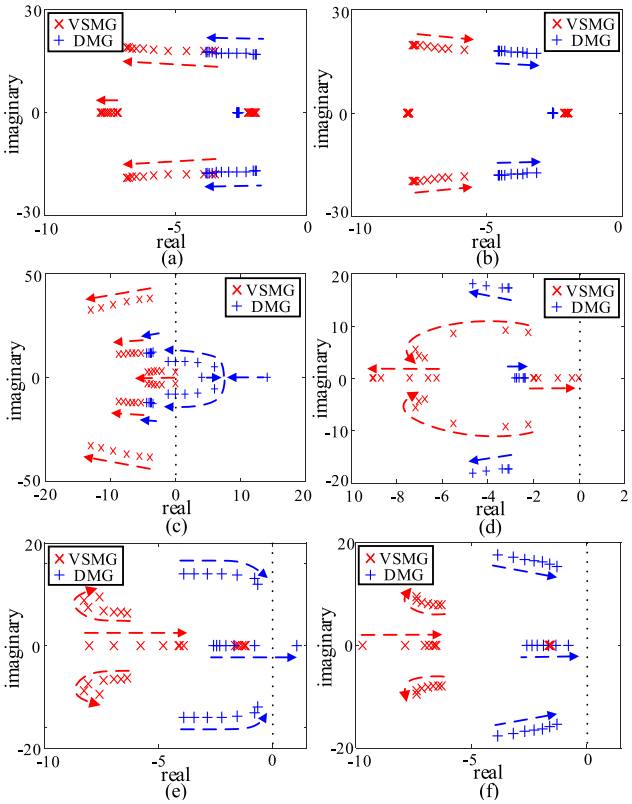

FIGURE 5. Eigenvalue trajectories of changing the local load, damping factors (droop coefficients) and virtual impedance parameters: (a) changing r_{load} from 0.1 to 5, (b) changing L_{load} from 1e-4 to 1e-2, (c) changing r_v from 0 to 2.8, (d) changing L_v from 2e-3 to 1.4e-2, (e) changing D_p from 5 to 10, (f) changing D_q from 6.5 to 1e4.

It can be observed form Fig. 5(a) and (b) that the variation of r_{load} or L_{load} has little effect on the dominant real eigenvalues for both microgrids, and their locations are very close in the s plane. As r_{load} increases, the dominant conjugate eigenvalues of both microgrids move toward the left, indicating increase of small-signal stabilities, whereas the growing L_{load} leads to the opposite situation. Besides, with the same r_{load} or L_{load}, dominant conjugate eigenvalues in the VSMG are distinctly farther from the imaginary axis than

those in the DMG, indicating better damping ratios in the dominant oscillation modes of VSMG.

Fig. 5(c) and (d) exhibit eigenvalue trajectories with damping factors D_p and D_q increasing (corresponding droop coefficients K_f and K_v are determined according to (10)). It can be seen from Fig. 5(c) that small-signal stabilities of both microgrids gradually increase with D_p growing. Under the premise of achieving the same steady-state droop effect, D_p in the VSMG has a larger stable region than K_f in the DMG. In Fig. 5(d), when $D_q = 6.5$, the DMG is small-signal unstable as there exists a pair of conjugate eigenvalues $(15 \pm i673)$ on the right half of the s plane (which are not shown in the figure since they are far from the origin), whereas the VSMG is small-signal stable. Then, as D_q increases, the DMG becomes small-signal stable, and the dominant real eigenvalues in both systems travel toward the unstable region, which indicates that small-signal stabilities of both microgrids are degraded. When $D_q = 1e4$, the DMG remains small-signal stable, whereas the VSMG becomes small-signal critical stable.

The reason why VSMG and DMG exhibit different stability with too small or too large D_q can be explained by analyzing (3) and (9). According to (3), the reactive power control of VSM is realized by detecting the terminal voltage deviation and adjusting the virtual internal electromotive force E. Besides, with the additional integral link, its output reactive power can be accurately controlled as $Q_e = Q_m + D_q(U - U_n)$. Thus, a relatively large D_q results in a large adjustment in E and a large deviation in Q_e, which is prone to cause instability, whereas a relatively small D_q can remain stable for the VSMG. According to (9), the reactive power control of droop control strategy is realized by detecting the output reactive power Q_e and adjusting the voltage reference E. A relatively small D_q results in a large adjustment in E, which is prone to cause instability, whereas a relatively large D_q can remain stable for the DMG. Even though the stable regions of D_q and K_v cannot be compared as they perform opposite stability at both ends of the parameters interval, the dominant conjugate eigenvalues in the VSMG have lower natural oscillation frequency and greater damping ratio compared to the DMG, which indicates the VSMG has better dynamic performance than the DMG under the same steady-state reactive power droop.

It can be observed from Fig. 5(e) and (f) that the effects of increasing r_v and L_v are similar. For the DMG, the increasing of virtual impedance (no matter r_v or L_v) introduces additional voltage drop and is equivalent to increasing K_v [27], i.e., decreasing D_q, so that eigenvalue trajectories of DMG are consistent with Fig. 5(d). However, for the VSMG, the additional voltage drop effect can be alleviated with the additional integral link in (3) by increasing E, so that the stability of VSMG is less sensitive to virtual impedance parameters, as indicated by the real dominant eigenvalues in Fig. 5(e) and (f). This also confirms that VSMG has wider stable regions for r_v and L_v than DMG. Hence, VSMG is significantly more robust against parameter variations and load uncertainties than DMG.

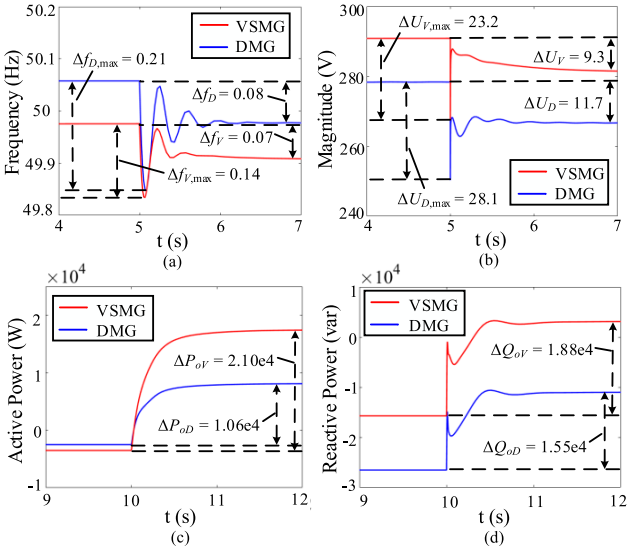

FIGURE 6. Time-domain responses of VSMG and DMG: (a) voltage frequency responses in the islanded operation, (b) voltage magnitude responses in the islanded operation, (c) output active power responses in the grid-connected operation, (d) output reactive power responses in the grid-connected operation.

B. TIME-DOMAIN ANALYSIS

Time-domain responses (obtained by simulation of nonlinear DAEs) of both kinds of microgrids are compared in both islanded and grid-connected operation. In the islanded operation, dynamic responses of voltage frequency and magnitude at Bus3 are compared under the local load changing from 25 + j10 kVA to 50 + j10 kVA at time $t = 5$s, as shown in Fig. 6(a) and (b). Before the load changes, the voltage frequency and magnitude in the VSMG are closer to nominal values, i.e., 50Hz and 311V, respectively. From Fig. 6(a), it can be seen that the maximum frequency drop of the VSMG is $\Delta f_{V,\max} = 0.14$Hz, while that of the DMG is $\Delta f_{D,\max} = 0.21$Hz. The steady-state frequency drop of the VSMG is $\Delta f_V = 0.07$Hz, while that of the DMG is $\Delta f_D = 0.08$Hz. The maximum absolute value of the rate of change of frequency (ROCOF) in the case of VSMG is 5.06Hz/s, while that of the DMG is 6.00Hz/s. From Fig. 6(b), it can be observed that the maximum voltage drop of the VSMG is $\Delta U_{V,\max} = 23.2$V, while that of the DMS is $\Delta U_{D,\max} = 28.1$V. The steady-state voltage drop of the VSMG is $\Delta U_V = 9.3$V, while that of the DMG is $\Delta U_D = 11.7$V. The deviations of voltage frequency and magnitude are smaller in the VSMG than in the DMG in both dynamic process and steady-state, which agrees with the frequency-domain analysis.

In the grid-connected operation, dynamic responses of output active and reactive power are compared under disturbances of ω_g and U_g. Figure 6(c) depicts dynamic responses of output active power with ω_g dropping 0.2πrad/s from the nominal value at $t = 10$s, where negative values mean the power is absorbed from the upstream network and vice versa. The variation of output active power in the VSMG ($\Delta P_{oV} = 21.0$kW) is greater than that in the DMG ($\Delta P_{oD} = 10.6$kW).

Note that before ω_g drops, the steady-state output active power of the VSMG is slightly smaller than that of the DMG. This is because the voltage magnitude at Bus3 is higher in the case of VSMG, which leads to a larger absorbed active power by the local load in the VSMG. Figure 6(d) shows dynamic responses of output reactive power with U_g dropping 0.1p.u. from the nominal value at $t = 10$s. The change of output reactive power in the VSMG ($\Delta Q_{oV} = 18.8$kvar) is greater than that in the DMG ($\Delta Q_{oD} = 15.5$kvar). It is clear that the VSMG provides more active and reactive power support than the DMG when voltage frequency and magnitude disturbances occur in the upstream network.

Time-domain comparisons indicate that VSMG performs better responses than DMG in both islanded and grid-connected operation. This is because, firstly, VSM control can be applied to both the supply side and the demand side. In the studied VSMG, both DER2 and the controllable load applying VSM control can automatically adjust their output power to reduce fluctuations of local voltage frequency and magnitude in the islanded operation and support the upstream network in the grid-connected operation, whereas only power supplies in the DMG can participate in the system regulation. Thus, VSMG have more satisfactory steady-state values than DMG. Secondly, in the case of reasonable design of virtual inertia parameters, the additional dynamics introduced by VSM control are coordinated with the inherent inertial dynamics of the SG, so as to reduce oscillations and smooth fluctuations in the dynamic process.

IV. MODEL ORDER REDUCTION OF THE VSMG

With the growing scale of VSMG, the order of its model will inevitably increase, so as the computational burdens of its analysis and simulation. In this Section, three representative MOR methods, i.e., BT, SP and PCPA methods are applied to the VSMG model.

A. MODEL ORDER REDUCTION BASED ON BALANCED TRANSFORMATION

Generally speaking, BT is a state coordinate transformation that makes the controllability and observability Grammians of the system identical and diagonal. Consider the small-signal VSMG model represented as (7), where A is assumed asymptotically stable, the pair (A, B) is assumed controllable and the pair (C, A) is assumed observable. The controllability and observability Grammians, denoted as P and Q, respectively, can be obtained by solving the Lyapunov equation:

$$\begin{cases} AP + PA^T + BB^T = 0 \\ A^T Q + QA + C^T C = 0 \end{cases} \tag{12}$$

It is known that there exists an invertible matrix T to obtain the balanced realization [28] of (7) as (Δ is omitted for simple expression):

$$\begin{cases} \dot{x}_b = A_b x_b + B_b u \\ y = C_b x_b + Du \end{cases} \tag{13}$$

where $x_b = Tx$, $A_b = TAT^{-1}$, $B_b = TB$, $C_b = CT$, with corresponding controllability and observability Grammians P_b and Q_b satisfying the following equation:

$$P_b = Q_b = \Sigma = diag\{\sigma_1, \sigma_2, \ldots, \sigma_N\}, \quad \sigma_1 \geq \sigma_2 \geq \ldots \geq \sigma_N > 0 \tag{14}$$

where σ_i is the so called Hankel singular value (HSV) and $\sigma_i = \sqrt{\lambda_i(PQ)}$. $\lambda_i(PQ)$ denotes the ith eigenvalue of PQ. The HSVs are important criteria in system MOR because they measure the contribution of each state to the input-output behavior. Detailed steps of obtaining T is elaborated in [29].

Assuming that the ratio:

$$\sum_{i=r+1}^{N} \sigma_i / \sum_{i=1}^{N} \sigma_i$$

is less than an acceptable small value, the states in (13) with indices from $r+1$ to N can be regarded having little contribution to dynamic responses and can be eliminated by considering corresponding dynamics equal to 0. Then the balanced VSMG model (13) can be rewritten in the partitioned quasi-steady-state format as:

$$x_b = \begin{bmatrix} x_{b1} \\ x_{b2} \end{bmatrix}, A_b = \begin{bmatrix} A_{11} & A_{12} \\ A_{21} & A_{22} \end{bmatrix},$$
$$B_b = \begin{bmatrix} B_{11} \\ B_{22} \end{bmatrix}, C_b = \begin{bmatrix} C_{11} & C_{22} \end{bmatrix},$$
$$\begin{cases} \dot{x}_{b1} = A_{11} x_{b1} + A_{12} x_{b2} + B_{11} u \\ 0 = A_{21} x_{b1} + A_{22} x_{b2} + B_{22} u \\ y = C_{11} x_{b1} + C_{22} x_{b2} + Du \end{cases} \tag{15}$$

where A_{11} is of dimension $r \times r$, and A_{22} is of $(N-r) \times (N-r)$, with remaining matrices having corresponding dimensions consistent with the system dimensions defined in (13). Even though the dynamics of x_{b2} are discarded, its steady-state gain can be remained by replacing (16) into (15).

$$x_{b2} = -A_{22}^{-1}(A_{21} x_{b1} + B_{22} u) \tag{16}$$

Thus, the reduced VSMG model can be derived as:

$$\begin{cases} \dot{x}_{b1} = A_r x_{b1} + B_r u \\ y = C_r x_{b1} + D_r u \end{cases} \tag{17}$$

where $A_r = A_{11} - A_{12}A_{22}^{-1}A_{21}$, $B_r = B_{11} - A_{12}A_{22}^{-1}B_{22}$, $C_r = C_{11} - C_{22}A_{22}^{-1}A_{21}$ and $D_r = D - C_{22}A_{22}^{-1}B_{22}$. Theoretically, BT method can reduce the system model to arbitrary order.

B. MODEL ORDER REDUCTION BASED ON SINGULAR PERTURBATION

The SP theory believes that the singular perturbed system can be decoupled into independent slow and fast subsystems, and the system reduction can be realized by neglecting the fast subsystem. For the VSMG with greater inertia than conventional microgrids, where slow dynamics are dominant, neglecting fast dynamics will have little influence in system responses. The VSMG model as (7) should be transformed

into the singularly perturbed format before applying the SP method. According to the participation factor analysis, rearrange state vector of (7) such that slow states x_1 are placed at upper rows and fast states x_2 are placed at lower rows, and the singularly perturbed presentation of (7) can be denoted as (Δ is omitted for simple expression):

$$\begin{cases} \dot{x}_1 = A_1 x_1 + A_2 x_2 + B_1 u \\ \varepsilon \dot{x}_2 = A_3 x_1 + A_4 x_2 + B_2 u \\ y = C_1 x_1 + C_2 x_2 + Du \end{cases} \tag{18}$$

where ε is a small positive singular perturbation parameter that indicates the separation between slow and fast states. Applying the Chang transformation, (18) can be decoupled into independent slow and fast subsystems as:

$$\begin{cases} \dot{z}_1 = A_s z_1 + B_s u \\ \varepsilon \dot{z}_2 = A_f z_2 + B_f u \\ y = C_s z_1 + C_f z_2 + Du \end{cases} \tag{19}$$

where z_1 and z_2 are decoupled slow and fast states, respectively; $A_s = A_1 - A_2 L$, $B_s = B_1 - MLB_1 - MB_2/\varepsilon$, $A_f = LA_2 + A_4/\varepsilon$, $B_f = LB_1 + B_2/\varepsilon$, $C_s = C_1 - C_2 L$, $C_f = C_2 - \varepsilon C_2 LM + \varepsilon C_1 M$, matrices L and M are introduced by Chang transformation and can be solved by iterations detailed in [17]. Since small ε is associated with the decoupled fast subsystem, (19) can be reduced as:

$$\begin{cases} \dot{z}_1 = A_s z_1 + B_s u \\ y = C_s z_1 + Du \end{cases} \tag{20}$$

The SP method decouples the original system into independent fast and slow subsystems by calculating "boundary layer" corrections in separate time scales [30]. Generally speaking, this method allows for proper inclusion of possible effect that fast states have on the slow subsystem. The model proposed in [19] was essentially the first iteration of L and M and deriving corresponding reduced microgrid model. Additionally, SP method can only reduce the VSMG model to certain orders where the states present distinct separation of time scales, otherwise matrices L and M cannot be solved.

C. MODEL ORDER REDUCTION BASED ON POLES CLUSTERING

The PCPA method is suitable to reduce systems represented by transfer functions. Most MOR methods for transfer function models simplify denominator and numerator polynomials separately. The traditional approach of denominator simplification mainly considers preserving stability between the original and reduced systems [31], such as Mihailov stability criterion [32], stability equation method [33], Routh approximation [34], etc. Instead, the poles clustering method engages all properties of the original system poles by agglomerative clustering depending on their distributions in the s plane. The numerator simplification considers the matching of time moments or Markov parameters, e.g., PA, or regards minimizing response errors between the original and reduced systems by heuristic optimization algorithms.

Since the PCPA method is applied to the transfer function model, the VSMG model as (7) should be firstly transformed into several single-input single-output (SISO) transfer functions. The procedure of poles clustering consists of the following steps:

1) Divide all the left half poles of the original transfer function into a certain number of clusters by the Euclidean distance based hierarchical poles clustering algorithm. The number of possible clusters determines the order of reduced system. Note that real and complex poles should be clustered separately.

2) Estimate a cluster-center for each cluster.

3) Improve the cluster-center according to the dominant pole of this cluster.

The detailed procedure is explained in [35]. Note that poles on the left half and the right half of the s plane are clustered separately, whereas poles on the imaginary axis or the origin should be retained in the reduced model.

After the poles clustering procedure, coefficients for the numerator are determined through the PA procedure. Expand the original transfer function $G(s)$ in Taylor series around $s = 0$ and $s = \infty$ respectively as:

$$\begin{aligned} G(s) &= \sum_{i=0}^{\infty} (T_{mi} s^i), \quad (\text{around } s = 0) \\ &= \sum_{i=0}^{\infty} (M_{ki} s^{-(i+1)}), \quad (\text{around } s = \infty) \end{aligned} \tag{21}$$

where T_{mi} and M_{ki} are the ith time moment and Markov parameter of $G(s)$, respectively. Consider the rth-order reduced model as:

$$G_r(s) = \frac{c_0 + c_1 s + c_2 s^2 \cdots + c_{r-1} s^{r-1}}{d_0 + d_1 s + d_2 s^2 \cdots + d_r s^r} \tag{22}$$

where c_i is the ith numerator coefficient of the reduced model and d_j is the jth denominator coefficient obtained by the poles clustering procedure. The coefficients of the reduced numerator are evaluated as:

$$\begin{cases} c_0 = d_0 T_{m0} \\ c_1 = d_0 T_{m1} + d_1 T_{m0} \\ \cdots \\ c_{\gamma-1} = d_0 T_{m(\gamma-1)} + d_1 T_{m(\gamma-2)} + \ldots + d_{\gamma-1} T_{m0} \\ c_{r-\beta} = d_r M_{k(\beta-1)} + d_{r-1} M_{k(\beta-2)} + \ldots + d_{r-\beta+1} M_{k0} \\ \cdots \\ c_{r-1} = d_r M_{k0} \end{cases} \tag{23}$$

where γ is the number of time moments and β is the number of Markov parameters. Therefore, all coefficients required for the reduced model as (22) are known.

V. EQUIVALENT SG MODEL OF THE VSMG

The participation factor analysis confirms that modes in group 1, which are low frequency oscillation modes with relatively large time constants and highly influencing the system stability, are mainly derived from states related to the

SG and VSM control loop. This inspires us that the VSMG model can be simplified into the structure of the SG model. The equivalent SG parameters of the VSMG can be obtained through the method of dynamic responses matching.

Similarly, in the field of power system model reduction, one of the most commonly used methods is coherency and aggregation. Coherency means that some SGs in a wide area exhibit similar rotor angle swings after a disturbance. Then the coherent groups of SGs can be aggregated into a single equivalent SG so as to simplify the system model. As for the microgrid, voltage angle differences of each node are not distinct in steady-state or under small disturbances. Besides, both DERs and controllable loads in the VSMG inherit output characteristics of synchronous machines. Inspired by the concept of coherency and aggregation, it is supposed that the VSMG model can be equivalent as an SG model. The EqSG model can be used in time-domain simulations and dynamic analysis of ADNs containing multi-VSMGs by substituting detailed VSMG models.

Dynamic equations of the EqSG model are based on the modified third-order SG model:

$$\begin{cases} \dot{\delta}^{eq} = \omega^{eq} - \omega_g \\ J^{eq}\dot{\omega}^{eq} = (P_{mg} - P_e^{eq})/\omega_n - D_p^{eq}(\omega^{eq} - \omega_g) \\ K^{eq}\dot{E}^{eq} = Q_{mg} - Q_e^{eq} - D_q^{eq}(U^{eq} - U_g) \end{cases} \tag{24}$$

The third-order EqSG model considers the excitation transient and rotor dynamics, where the superscript eq denotes corresponding equivalent variable or parameter of the VSMG, P_{mg} and Q_{mg} are active and reactive power instructions derived by the microgrid secondary control, respectively; P_e^{eq} and Q_e^{eq} are internal active and reactive power of the EqSG, respectively, which can be calculated by the following equations:

$$\begin{cases} P_e^{eq} = 1.5[(E^{eq})^2 \cos\alpha - E^{eq}U_g \cos(\delta^{eq} + \alpha)]/Z \\ Q_e^{eq} = 1.5[(E^{eq})^2 \sin\alpha - E^{eq}U_g \sin(\delta^{eq} + \alpha)]/Z \end{cases} \tag{25}$$

where Z is the equivalent impedance from the EqSG to the upstream network and α is the impedance angle. Note that each VSM in the VSMG cannot sample the PCC voltage and its output reactive power is directly influenced by the capacitor voltage of its LC filter, so the internal sampling voltage, denoted as U^{eq} in (24), is introduced.

$$U^{eq} = (1 - r_x)E^{eq} + r_x U_g, \quad 0 < r_x < 1 \tag{26}$$

The EqSG model is proposed for grid-connected VSMG. Thus, ω_g and U_g are input signals. The output active and reactive power, denoted as P_o and Q_o, are defined as output signals:

$$\begin{cases} P_o = 1.5[E^{eq}U_g \cos(\alpha - \delta^{eq}) - {U_g}^2 \cos\alpha]/Z \\ Q_o = 1.5[E^{eq}U_g \sin(\alpha - \delta^{eq}) - {U_g}^2 \sin\alpha]/Z \end{cases} \tag{27}$$

The structure of the EqSG model is defined through (24)-(27), and the complete EqSG model can be obtained by determining the following 7 equivalent parameters, i.e., J^{eq}, D_p^{eq}, K^{eq}, D_q^{eq}, Z, α, and r_x. In this paper, these equivalent parameters are determined by matching dynamic responses of the EqSG model with the complete VSMG small-signal model, which can also be recognized as gray-box system identification. Since the equivalent model is effective under small disturbances, the linearized EqSG model is used in the equivalencing procedure, which can also speed up the gray-box system identification. The linearized EqSG model can be presented in the state-space format:

$$\begin{cases} \Delta x_{eq} = A_{eq}\Delta x_{eq} + B_{eq}\Delta u \\ \Delta y = C_{eq}\Delta x_{eq} + D_{eq}\Delta u \end{cases} \tag{28}$$

where $\Delta x_{eq} = [\Delta\delta^{eq}, \Delta\omega^{eq}, \Delta E^{eq}]^T$, $\Delta u = \left[\Delta\omega_g, \Delta U_g\right]^T$, $\Delta y = [\Delta P_o, \Delta Q_o]^T$, state-space matrices A_{eq}, B_{eq}, C_{eq} and D_{eq} are displayed in Appendix C. The equivalencing procedure is illustrated by the flowchart in Fig. 7.

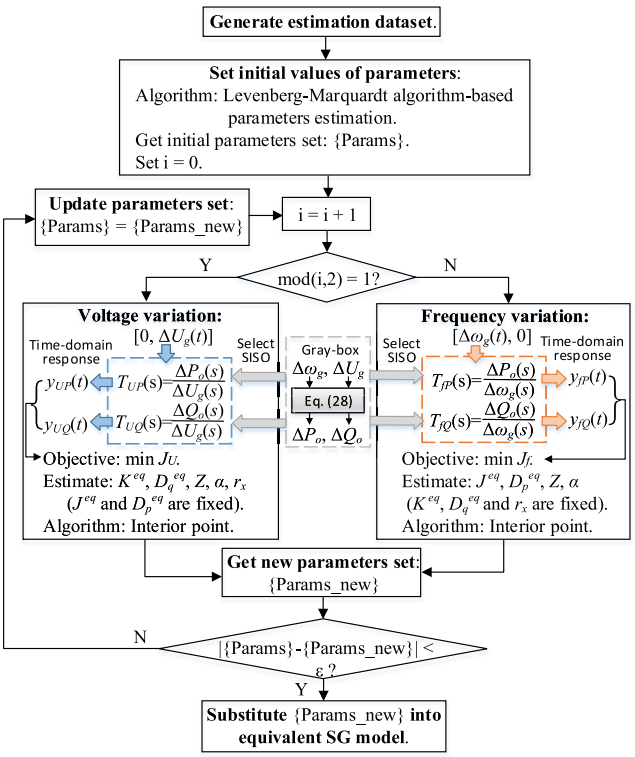

FIGURE 7. Flowchart of the equivalencing procedure.

1) STEP 1: CREATE ESTIMATION DATA

Since the EqSG model is studied in the small-signal region, fluctuations in the input signals should satisfy the meaning of small disturbances in power systems. According to "GB/T12325-2008" and "GB/T15945-2008", fluctuations of voltage magnitude and frequency in power systems should not exceed ±5% and ±0.2Hz, respectively, which can be regarded as the range of small disturbances. In order to improve the applicability of estimated equivalent parameters, fluctuations in the input signals of estimation data reach their extreme values of the small-signal region in the form of step changes. The output signals of estimation data

are dynamic responses derived from the small-signal grid-connected VSMG model according to input signals of estimation data. Thus, the estimation data can be collected into 3 sets as summarized in Table 1.

TABLE 1. Estimation dataset.

No.	Input Signals	Output Signals
1	$[\Delta\omega_g(t), \Delta U_g(t)]$	$[\Delta P_{oV1}(t), \Delta Q_{oV1}(t)]$
2	$[0, \Delta U_g(t)]$	$[\Delta P_{oV2}(t), \Delta Q_{oV2}(t)]$
3	$[\Delta\omega_g(t), 0]$	$[\Delta P_{oV3}(t), \Delta Q_{oV3}(t)]$

2) STEP 2: SET INITIAL VALUES OF EQUIVALENT PARAMETERS

The System Identification Toolbox in MATLAB was used to create the linear EqSG gray-box model (28). The initial values of equivalent parameters are obtained by an once Levenberg-Marquardt algorithm based parameters estimation with estimation dataset 1. The goal is to determine proper initial values of unknown equivalent parameters by minimizing the sum of squared errors between $[\Delta P_{oV1}(t), \Delta Q_{oV1}(t)]$ and time-domain responses of the gray-box model (28).

3) STEP 3: ESTIMATE EQUIVALENT PARAMETERS ALTERNATELY AND ITERATIVELY

Due to the coupling of output active and reactive power in the low-voltage VSMG, the estimated parameters derived from estimation dataset 1 are only effective within a narrow range of input signals. For the linearized EqSG model, dynamic responses of multi-inputs can be dealt with the sum of each SISO response. Thus, the estimation procedure is subdivided into two parts, i.e., the voltage-variation response estimation and the frequency-variation response estimation. These two subprocesses are executed alternately and iteratively until the unknown equivalent parameters convergence, so that the estimated parameters will satisfy a wide range of input signals.

In the voltage-variation response estimation, the estimation dataset 2 is used, in which step changes occur in U_g while ω_g remains unchanged in the input signals. To obtain output responses faster, the gray-box model (28) is separated into two SISO transfer functions, denoted as $T_{UP}(s)$ and $T_{UQ}(s)$, respectively. From (24), it's clear that J^{eq} and D_p^{eq} mainly influence the response of output active power when ω_g changes, whereas K^{eq}, D_q^{eq} and r_x primarily affect the response of output reactive power when U_g changes. Thus, in the voltage-variation response estimation, K^{eq}, D_q^{eq}, Z, α, and r_x are allowed to change while other parameters (J^{eq} and D_p^{eq}) are fixed.

Similarly, in the frequency-variation response estimation, the estimation dataset 3 is adopted. The gray-box model (28) is separated as $T_{fP}(s)$ and $T_{fQ}(s)$ where J^{eq}, D_p^{eq}, Z and α are able to change while other parameters (K^{eq}, D_q^{eq} and r_x) are constant.

In each iteration, parameters allowed to change are updated by minimizing the objective function J_U (for voltage-variation response estimation) or J_f (for frequency-variation response estimation) through interior point algorithm, which can be fulfilled with MATLAB Optimization Toolbox. The objective functions are weighted square average errors between time-domain responses of the estimated model and output signals of the estimation data:

$$J_U = w_{UP}\sqrt{\frac{1}{N_s}\sum_{i=1}^{N_s}[\Delta P_{oV2}(t_i) - y_{UP}(t_i)]^2} + w_{UQ}\sqrt{\frac{1}{N_s}\sum_{i=1}^{N_s}[\Delta Q_{oV2}(t_i) - y_{UQ}(t_i)]^2} \quad (29)$$

$$J_f = w_{fP}\sqrt{\frac{1}{N_s}\sum_{i=1}^{N_s}[\Delta P_{oV3}(t_i) - y_{fP}(t_i)]^2} + w_{fQ}\sqrt{\frac{1}{N_s}\sum_{i=1}^{N_s}[\Delta Q_{oV3}(t_i) - y_{fQ}(t_i)]^2} \quad (30)$$

where $y_{UP}(t)$ and $y_{UQ}(t)$ are time-domain responses of $T_{UP}(s)$ and $T_{UQ}(s)$ with input signals of estimation dataset 2, respectively; $y_{fP}(t)$ and $y_{fQ}(t)$ are time-domain responses of $T_{fP}(s)$ and $T_{fQ}(s)$ with input signals of estimation dataset 3, respectively; N_s is the number of sampling points; w_{UP}, w_{UQ}, w_{fP} and w_{fQ} are weight coefficients and $w_{UP} = w_{fQ} = 0.2$, $w_{UQ} = w_{fP} = 0.8$.

After the parameters convergence, the EqSG model is obtained by updating the estimated parameters in (28).

VI. CASE STUDIES

Three MOR methods mentioned in Section IV and the proposed EqSG method are compared with each other in the studied grid-connected VSMG, so as to summarize their advantages and disadvantages in the application of microgrid model reduction. The input signals for testing different MOR methods are described in Table 2, where disturbances occur in ω_g and U_g respectively. The amplitudes of disturbances are 50% of their extreme values of the small-signal region. Since the proposed EqSG method fixes the reduced VSMG model into third-order, reduced models derived from BT and PCPA are also restricted to third-order for a fair comparison. Note that the reduced model derived from SP is a fourth-order model as the slow and fast subsystems of the studied VSMG cannot be decoupled at third-order. Reduced models derived by three MOR methods and equivalent parameters derived from the EqSG method are displayed in Appendix C.

TABLE 2. Test input signals.

No.	$\Delta\omega_g(t)$	$\Delta U_g(t)$
1	$\begin{cases} 0, & t \in [0,1) \cup (3,5] \\ 0.1 * 2\pi, & t \in [1,3] \end{cases}$	0
2	0	$\begin{cases} 0, & t \in [0,1) \cup (3,5] \\ 2.5\% * U_n, & t \in [1,3] \end{cases}$

Fig. 8 compares frequency-domain characteristics of f-P responses among the reduced-order models. It can be observed form Fig. 8(a) that all of the four MOR methods provide excellent matching with the full-order VSMG small-signal model in low frequency band (0-10rad/s). The EqSG method provides the widest frequency band (0-450rad/s) in properly approximating to the full-order model among four MOR methods. Both BT and SP methods exhibit obvious truncation characteristics because they both eliminate high frequency modes to some extent, but the properly matched frequency range of BT method (0-305rad/s) is larger than that of SP method (0-25rad/s). The PCPA method does not show truncation characteristics. The slope of PCPA method in high frequency band ($>1e4$ rad/s) is the same with that of the full-order model (-20dB/dec), but its amplitude response presents apparent difference with the original model from the corner frequency (10rad/s). This is because PCPA method is able to preserve high frequency poles, but the clustered high frequency poles are modified according to the dominant poles to preserve slow dynamics preferably, which leads to a slope match but amplitude mismatch in the high frequency domain. Figure 8(b) depicts phase-frequency characteristics of f-P responses, where BT method performs a better approximation to the full-order model than other methods while the SP method exhibits the worst matching.

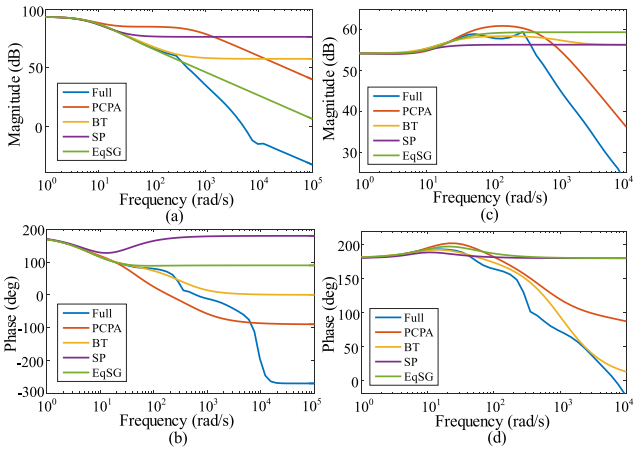

FIGURE 8. **Frequency-domain responses among 4 different MOR methods: (a) amplitude-frequency characteristics of f-P responses, (b) phase-frequency characteristics of f-P responses, (c) amplitude-frequency characteristics of V-Q responses, (d) phase-frequency characteristics of V-Q responses.**

Fig. 8(c) and (d) depict amplitude-frequency and phase-frequency characteristics of V-Q responses, respectively. It can be observed from Fig. 8(c) that PCPA method performs better approximation in high frequency band ($>1e3$ rad/s) than other MOR methods, because the slope of PCPA method is the same with the full-order model in high frequency band while other MOR methods exhibit high frequency truncation characteristics. There are mainly two reasons. Firstly, the V-Q response is generally faster than the f-P response. The elimination of some high frequency dynamics caused by BT, SP and EqSG methods will inevitably reduce the proximity in the V-Q response. Secondly, PCPA method is based on the transfer function model, which can provide the reduced model for the V-Q response independently, and the clustering of poles is not affected by other input-output responses. But in low-mid frequency band (0-360rad/s), BT and EqSG methods perform better approximation than SP and PCPA methods. From Fig. 8(d), it can be observed that BT method performs better approximation than other MOR methods in the phase-frequency characteristic.

Note that, in the f-P response, the full-order model is a minimum phase system, reduced models derived by PCPA and EqSG are also minimum phase systems, while reduced models derived by BT and SP are non-minimum phase systems. In the V-Q response, the full-order system is a non-minimum phase system and all reduced models are also non-minimum phase systems. This indicates that PCPA and EqSG methods are better than BT and SP in maintaining the structural properties of the original system.

Further, a comparison of time-domain dynamic responses is analyzed and shown in Fig. 9. It can be seen from Fig. 9(a) and (c) that all methods match well with the full-order model in the steady-state. Whereas in the transient process, for the f-P response, PCPA and SP methods show relatively larger response errors than BT and EqSG methods, as shown in Fig. 9(b). For the V-Q response, shown as Fig. 9(d), all methods fail to precisely match with the high frequency oscillations of the full-order model in the transient process. But the EqSG method performs better matching than other three MOR methods. To compare the matching degrees of different MOR methods in a quantitative way, the normalized root-mean-square error (NRMSE) is chosen as the index for evaluation of matching degrees:

$$\mathrm{NRMSE} = \left(1 - \frac{\left\|y_o - \hat{y}_r\right\|_2}{\left\|y_o - \bar{y}_o\right\|_2}\right) \times 100\% \tag{31}$$

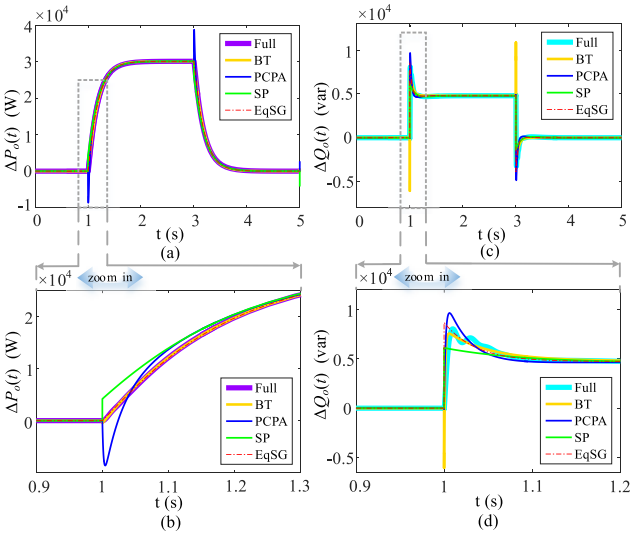

FIGURE 9. **Time-domain dynamic responses of 4 different MOR methods: (a) whole process of f-P responses, (b) transient process f-P responses, (c) whole process of V-Q responses, (d) transient process of V-Q responses.**

where y_o denotes the dynamic response of the full-order model, $\hat{y}_r$ is the time-domain response derived by the reduced model and $\bar{y}_o$ is the mean of y_o. Table 3 lists matching degrees of different MOR methods with different input signals. It is clear that EqSG method performs the best matching effect among four MOR methods.

TABLE 3. Matching degrees of 4 MOR methods.

MOR method	Matching of f-P responses	Matching of V-Q responses
BT	98.76%	32.96%
SP	81.28%	7.54%
PCPA	76.22%	55.93%
EqSG	99.41%	84.32%

Table 4 compares different properties of four MOR methods in VSMG model reduction, where the EqSG method shows more superiorities than other MOR methods. The EqSG method is suitable for both state-space model and transfer function model because it is based on dynamic equivalence of the original model. The EqSG method performs the best matching in low frequency of amplitude-frequency characteristics and has the best fitting degree in time-domain responses. Besides, this method maintains identical type of phase system with the original model. As for the stability consistency, BT and SP methods satisfy stability consistency because they require the original model to be asymptotically stable and their procedures are essentially linear transformations of state matrices which will not change system stability. The PCPA method preserves stability consistency because the poles on both sides of the s plane are clustered separately. The EqSG method also retains stability consistency because this method correctly fits output signals of the estimation data which reflects stability of the original system. Furthermore, the most significant advantage of the EqSG method is to keep equivalent physical meanings in the reduced states and provides equivalent electrical parameters which are instructive in power system analysis.

TABLE 4. Properties comparison of 4 MOR methods in VSMG model reduction.

Properties	BT	SP	PCPA	EqSG
Model format	MIMO state space model.	MIMO state space model.	SISO transfer function.	Both.
Principle	Rearrangement of states according to states' energy and elimination of minor states.	Decoupling of fast and slow subsystem and elimination of fast subsystem.	Poles clustering for denominator and Padé approximation for numerator.	Gray-box system identification and equivalent parameters estimation.
Reduction order	Arbitrary order.	Depend on distribution of HSVs.	Depend on distribution of poles.	Fix to third-order.
Matching of amplitude-frequency characteristics.	Good in low frequency.	Relatively good in low frequency.	Relatively good in low frequency.	Best in low frequency.
	Exhibit truncation in high frequency.	Exhibit truncation in high frequency.	Good in slope of high frequency.	Exhibit truncation in high frequency.
Matching of phase-frequency characteristics.	Good.	Poor.	Relatively good.	Relatively good.
Matching of time domain responses.	Good in steady state but poor in transient process.	Good in steady state but poor in transient process.	Good in steady state but poor in transient process.	Good in steady state and transient process.
Consistency in the type of phase system.	May be inconsistent.	May be inconsistent.	Consistent.	Consistent.
Consistency in stability.	Consistent. (Require original model stable.)	Consistent. (Require original model stable.)	Consistent.	Consistent.
States meaning	Lose inherent physical meanings.	Lose inherent physical meanings.	Lose inherent physical meanings.	Have equivalent physical meanings.

To further verify the effectiveness of EgSG model substituting detailed VSMG model in power system simulations, historical PCC frequency and voltage data of an actual microgrid, shown as Fig. 10 (where nominal values are subtracted to show fluctuations), is applied to the derived EqSG model, and corresponding time-domain responses are compared with simulation responses of the detailed VSMG (illustrated as Fig. 1) obtained through MATLAB/Simulink.

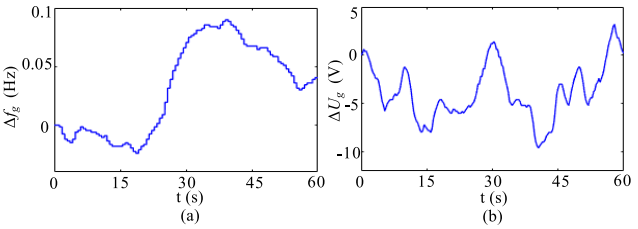

FIGURE 10. Historical data at PCC of an actual microgrid: (a) frequency variation waveform, (b) voltage magnitude variation waveform.

In this case study, fluctuations of ω_g and U_g are applied simultaneously to be consistent with the actual situation. It can be observed from Fig. 11 that responses of the EqSG model properly match with the detailed VSMG model (output active and reactive power values at nominal ω_g and U_g are subtracted in detailed VSMG's waveforms). Matching degrees of the EqSG model calculated according to (31) are 96.12% for output active power response and 97.93%

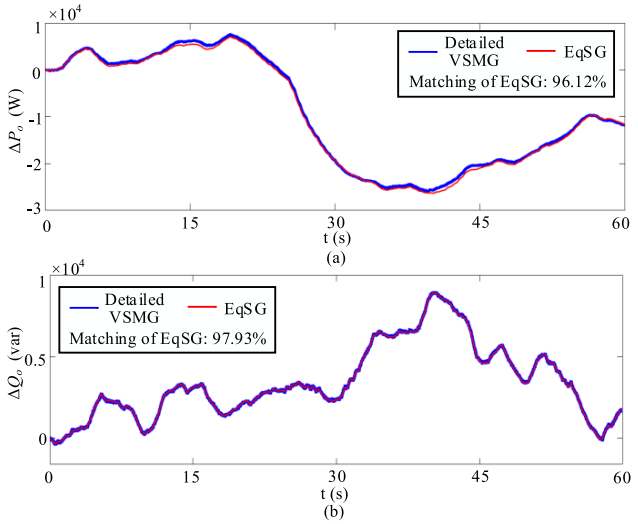

FIGURE 11. Responses comparison between the EqSG model and the detailed VSMG model: (a) output active power response waveform, (b) output reactive power response waveform.

for output reactive power response in this case study. Since step changes seldom occur in ω_g and U_g in actual operation, matching degrees in this case are better than those listed in Table 3. As the variation of U_g inevitably influences active power in low-voltage microgrids, output active power of the EqSG model exhibits slightly error compared with the detailed VSMG when the variation of U_g is relatively large, as shown in Fig. 11(a), so that the matching degree of active power response is slightly lower than the reactive power response in this case. Note that in order to ensure the accuracy of the EqSG model, disturbances in the input signals should not exceed the small-signal region ($\pm$0.2Hz in frequency and $\pm$5% in voltage), as the equivalent parameters are obtained based on the small-signal model of the VSMG.

VII. CONCLUSION

This paper compares dynamic characteristics between VSMG and DMG. With additional inertia dynamics and proper inertia parameters, the VSMG exhibits better dynamic characteristics than DMG in both islanded and grid-connected operations. In the islanded operation, the VSMG is more robust against parameter variations, and performs less disturbance in transient process and faster recovery to steady-state when the local load changes. In the grid-connected operation, the VSMG provides more power support to the upstream network than DMG when voltage or frequency fluctuates at PCC.

The participation factor analysis indicates that static stability and dynamic characteristics of the VSMG are mainly influenced by states associated with the SG and VSM control loop. According to this, the third-order EqSG model is proposed to reduce the VSMG model. The EqSG method applies gray-box system identification and is effective in the small-signal region. To speed up the gray-box system identification, linearized EqSG model is used in the equivalencing procedure. To improve the matching degree of output responses, the equivalencing is subdivided into different input-output responses estimation and estimates equivalent parameters alternately and iteratively. The EqSG model shows more superiorities than BT, SP and PCPA methods in both frequency-domain and time-domain. It can be used in dynamic analysis and time-domain simulations of power systems containing multi-VSMGs, as its dynamic responses properly match with the detailed VSMG model. In addition, the EqSG model preserves equivalent physical meaning in reduced states and provides equivalent electrical parameters for power system analysis.

APPENDIX A

Equations for modeling the voltage current dual-loop control are expressed as:

$$\dot{x}_d = v_{cd} - {v_{cd}}^*, \quad \dot{x}_q = v_{cq} - {v_{cq}}^* \tag{32}$$

$${i_{fd}}^* = K_{pv}\dot{x}_d + K_{iv}x_d, \quad {i_{fq}}^* = K_{pv}\dot{x}_q + K_{iv}x_q \tag{33}$$

$$y_d = i_{fd} - {i_{fd}}^*, \quad y_q = i_{fq} - {i_{fq}}^* \tag{34}$$

$$\begin{cases} {v_d}^* = K_{pi}\dot{y}_d + K_{ii}y_d - \omega L_f i_{fq} \\ {v_q}^* = K_{pi}\dot{y}_q + K_{ii}y_q + \omega L_f i_{fd} \end{cases} \tag{35}$$

where ${i_{fd}}^*$ and ${i_{fq}}^*$ are inductor current references of the LC filter; i_{fd} and i_{fq} are inductor current measurements of the LC filter; ${v_d}^*$ and ${v_d}^*$ are output voltage references of the converter; K_{pv}, K_{iv}, K_{pi} and K_{ii} are proportional gains and integral gains of the voltage controller and the current controller, respectively; x_d, x_q, y_d and y_q are states introduced by integral controllers.

Due to the realization of high switching frequencies, SVPWM and switching process of the converter can be neglected, and the converter can be regarded as a proportional link with gain K_{inv}. For convenience, a gain $K_g = 1/K_{inv}$ is introduced to make the output voltage of the converter (v_d, v_q) equal to its reference.

$$\begin{cases} v_d = K_{inv}K_g{v_d}^* = {v_d}^* \\ v_q = K_{inv}K_g{v_q}^* = {v_q}^* \end{cases} \tag{36}$$

The nonlinear model of the LC filter can be represented as:

$$\begin{cases} \dot{i}_{fd} = \left[(v_d - v_{cd}) - r_f i_{fd}\right]/L_f + \omega i_{fq} \\ \dot{i}_{fq} = \left[(v_q - v_{cq}) - r_f i_{fq}\right]/L_f - \omega i_{fd} \end{cases} \tag{37}$$

$$\begin{cases} \dot{v}_{cd} = (i_{fd} - i_{od})/C_f + \omega v_{cq} \\ \dot{v}_{cq} = (i_{fq} - i_{oq})/C_f - \omega v_{cd} \end{cases} \tag{38}$$

where r_f is the parasitic resistance of inductor L_f, and C_f denotes the shunt capacitor.

Modeling of the network and the local load is represented in the common rotational reference frame (DQ-axis) of the whole microgrid system. For generality, the dq-axis frame of DER1, whose angular velocity is denoted as ω_r, is chosen as the DQ-axis frame. Subscript D or Q appeared in the following voltages and currents represents corresponding D or Q axis component. The transformation equations between dq-axis frame and DQ-axis frame are expressed as:

$$\dot{\delta}_i = \omega_i - \omega_r \tag{39}$$

$$\begin{cases} v_{bD,i} = v_{cd,i}\cos\delta_i - v_{cq,i}\sin\delta_i \\ v_{bQ,i} = v_{cd,i}\sin\delta_i + v_{cq,i}\cos\delta_i \end{cases} \tag{40}$$

$$\begin{cases} i_{od,i} = i_{lineD,ij}\cos\delta_i + i_{lineQ,ij}\sin\delta_i \\ i_{oq,i} = -i_{lineD,ij}\sin\delta_i + i_{lineQ,ij}\cos\delta_i \end{cases} \tag{41}$$

where the subscript i (or j) denotes the ith (or jth) Bus, the subscript ij denotes the connection between Bus$i$ and Bus$j$, δ_i is the angle of Bus$i$'s dq-axis frame with respect to the DQ-axis frame, $v_{bD,i}$ and $v_{bQ,i}$ are voltages of Bus$i$, $i_{lineD,ij}$ and $i_{lineQ,ij}$ are currents of Lineij.

The RL branch model is adopted for the network because the equivalent capacitance to ground of the line can be ignored in microgrids.

$$\begin{cases} \dot{i}_{lineD,ij} = (v_{bD,i} - v_{bD,j} - r_{line,ij}i_{lineD,ij})/L_{line.ij} \\ \qquad + \omega_r i_{lineQ,ij} \\ \dot{i}_{lineQ,ij} = (v_{bQ,i} - v_{bQ,j} - r_{line,ij}i_{lineQ,ij})/L_{line,ij} \\ \qquad - \omega_r i_{lineD,ij} \end{cases} \tag{42}$$

where $r_{line,ij}$ and $L_{line,ij}$ are resistance and inductance of Lineij respectively.

The local load is considered as the combination of resistor r_{load} and inductor L_{load} so as to reflect the load dynamics.

$$\begin{cases} \dot{i}_{loadD} = (v_{bD,i} - r_{load} i_{loadD})/L_{load} + \omega_r i_{loadQ} \\ \dot{i}_{loadQ} = (v_{bQ,i} - r_{load} i_{loadQ})/L_{load} - \omega_r i_{loadD} \end{cases} \tag{43}$$

where i_{loadD} and i_{loadQ} are currents of the local load.

Since there is no corresponding output variable to provide voltage value for the node that is not directly connected to a capacitor, a virtual resistor r_N is assumed between this type of node and ground to determine the voltage value. The value of r_N should be sufficiently large such that its introduction has minimum influence on the system stability.

$$\begin{cases} v_{bD,j} = r_N \left(\sum_{i=0}^{i \neq j} i_{lineD,ij} - i_{loadD} \right) \\ v_{bQ,j} = r_N \left(\sum_{i=0}^{i \neq j} i_{lineQ,ij} - i_{loadQ} \right) \end{cases} \tag{44}$$

For the grid-connected VSMG, the input variable U_g should also be transformed in the DQ-axis frame to integrate into the microgrid model:

$$\dot{\delta}_g = \omega_g - \omega_r \tag{45}$$

$$\begin{cases} v_{gD} = U_g \cos \delta_g \\ v_{gQ} = U_g \sin \delta_g \end{cases} \tag{46}$$

where δ_g is the angle of the upstream grid's rotational reference frame with respect to the DQ-axis frame, v_{gD} and v_{gQ} are grid voltages represented in the DQ-axis frame.

Also, dynamics of the grid-connection line with resistance r_g and inductance L_g should be included in the grid-connected VSMG model.

$$\begin{cases} \dot{i}_{gD} = (v_{bD,i} - v_{gD} - r_g i_{gD})/L_g + \omega_r i_{gQ} \\ \dot{i}_{gQ} = (v_{bQ,i} - v_{gQ} - r_g i_{gQ})/L_g - \omega_r i_{gD} \end{cases} \tag{47}$$

where i_{gD} and i_{gQ} are grid-connected currents of the VSMG.

System parameters of the VSMG are listed in Table 5. For the convenience of analysis, control parameters of each VSM are the same.

TABLE 5. System parameters.

Parameter	Value	Parameter	Value
J(W·s^3/rad^2)	0.093	D_p(W·s^2/rad^2)	50.66
K(var·s/V)	0.15	D_q(var/V)	321.4
K_{pv}	0.5	K_{iv}	400
K_{pi}	10	K_{ii}	15000
$r_f(\Omega)$	0.1	L_f(mH)	2
C_f(uF)	50	$r_N(\Omega)$	5000
$r_g(\Omega)$	0.1	L_g(mH)	0.5
$r_{line,03}(\Omega)$	0.15	$L_{line,03}$(mH)	0.4
$r_{line,13}(\Omega)$	0.1	$L_{line,13}$(mH)	0.5
$r_{line,23}(\Omega)$	0.2	$L_{line,23}$(mH)	0.6

APPENDIX B

Eigenvalues and corresponding participation factors are listed in Table 6.

APPENDIX C

The state-space matrices A_{eq}, B_{eq}, C_{eq} and D_{eq} are:

$$A_{eq} = \begin{bmatrix} 0 & 1 & 0 \\ -\dfrac{K_{Pe\delta}}{J^{eq}\omega_n} & -\dfrac{D_p^{eq}}{J^{eq}} & -\dfrac{K_{PeE}}{J^{eq}\omega_n} \\ -K^{eq}K_{Qe\delta} & 0 & K_A \end{bmatrix}$$

$$B_{eq} = \begin{bmatrix} -1 & 0 \\ 0 & -\dfrac{K_{PeU}}{J^{eq}\omega_n} \\ 0 & -K^{eq}(D_q^{eq} r_x + K_{QeU}) \end{bmatrix}$$

$$C_{eq} = \begin{bmatrix} K_{Po\delta} & 0 & K_{PoE} \\ K_{Qo\delta} & 0 & K_{QoE} \end{bmatrix}, \quad D_{eq} = \begin{bmatrix} 0 & K_{PoU} \\ 0 & K_{QoU} \end{bmatrix}$$

where

$$\begin{aligned} K_A &= -K^{eq}[D_q^{eq}(1 - r_x) + K_{QeE}] \\ K_{Pe\delta} &= \partial P_e^{eq}/\partial \delta^{eq} = 1.5E_0^{eq} U_{g0} \sin(\delta_0^{eq} + \alpha)/Z, \\ K_{PeE} &= \partial P_e^{eq}/\partial E^{eq} \\ &= 1.5[2E_0^{eq} \cos\alpha - U_{g0} \cos(\delta_0^{eq} + \alpha)]/Z, \\ K_{PeU} &= \partial P_e^{eq}/\partial U_g = -1.5E_0^{eq} \cos(\delta_0^{eq} + \alpha)/Z, \\ K_{Qe\delta} &= \partial Q_e^{eq}/\partial \delta^{eq} = -1.5E_0^{eq} U_{g0} \cos(\delta_0^{eq} + \alpha)/Z, \\ K_{QeE} &= \partial Q_e^{eq}/\partial E^{eq} \\ &= 1.5[2E_0^{eq} \sin\alpha - U_{g0} \sin(\delta_0^{eq} + \alpha)]/Z, \\ K_{QeU} &= \partial Q_e^{eq}/\partial U_g = -1.5E_0^{eq} \sin(\delta_0^{eq} + \alpha)/Z, \\ K_{Po\delta} &= \partial P_o/\partial \delta^{eq} = 1.5E_0^{eq} U_{g0} \sin(\alpha - \delta_0^{eq})/Z, \\ K_{PoE} &= \partial P_o/\partial E^{eq} = 1.5U_{g0} \cos(\alpha - \delta_0^{eq})/Z, \\ K_{PoU} &= \partial P_o/\partial U_g \\ &= 1.5[E_0^{eq} \cos(\alpha - \delta_0^{eq}) - 2U_{g0} \cos\alpha]/Z, \\ K_{Qo\delta} &= \partial Q_o/\partial \delta^{eq} = -1.5E_0^{eq} U_{g0} \cos(\alpha - \delta_0^{eq})/Z, \\ K_{QoE} &= \partial Q_o/\partial E^{eq} = 1.5U_{g0} \sin(\alpha - \delta_0^{eq})/Z, \\ K_{QoU} &= \partial Q_o/\partial U_g \\ &= 1.5[E_0^{eq} \sin(\alpha - \delta_0^{eq}) - 2U_{g0} \sin\alpha]/Z \end{aligned}$$

where U_{g0} is the measured initial value of U_g, E_0^{eq} and δ_0^{eq} can be calculated according to (27) with measured initial values of output active and reactive power of the VSMG.

Reduced model derived from BT method:

$$A_r = \begin{bmatrix} -5.403 & -0.2736 & -0.7535 \\ 7.700 & -109.9 & 331.2 \\ -6.607 & 222.8 & -845.4 \end{bmatrix}$$

$$B_r = \begin{bmatrix} -517.8 & 2.844 \\ 366.1 & -397.5 \\ -311.8 & 1.077e3 \end{bmatrix}$$

TABLE 6. System eigenvalues.

	Eigenvalue real part	Eigenvalue imag part	Natural frequency (rad/s)	Damping ratio	Time constant (s)	Most Related states	Group No.
λ_1	-1.77	0	1.77	1	5.66E-01	δ_3	1
λ_2	-8.55	0	8.55	1	1.17E-01	δ_2	
$\lambda_{3,4}$	-6.93	±8.24	10.77	0.64	1.44E-01	v_f(SG), φ_{fd}(SG)	
$\lambda_{5,6}$	-6.13	±18.47	19.46	0.32	1.63E-01	ω_r(SG), p_m(SG)	
λ_7	-33.17	0	33.17	1	3.02E-02	φ_{kq}(SG), P_e	
$\lambda_{8,9}$	-42.26	±12.61	44.10	0.96	2.37E-02		
$\lambda_{10,11}$	-29.16	±37.63	47.61	0.61	3.43E-02	Q_e, E	
$\lambda_{12,13}$	-43.21	±33.04	54.40	0.79	2.31E-02		
λ_{14}	-73.98	0	73.98	1	1.35E-02	ω	
λ_{15}	-99.42	0	99.42	1	1.01E-02		
λ_{16}	-128.83	0	128.83	1	7.76E-03	φ_{kd}(SG)	
$\lambda_{17,18}$	-200.66	±315.64	374.02	0.54	4.98E-03	x_d, x_q	
$\lambda_{19,20}$	-248.01	±326.73	410.20	0.60	4.03E-03		
$\lambda_{21,22}$	-811.90	±0.77	811.90	1.00	1.23E-03	y_d, y_q	2
$\lambda_{23,24}$	-811.91	±2.47	811.91	1.00	1.23E-03		
$\lambda_{25,26}$	-803.88	±187.05	825.35	0.97	1.24E-03	$\varphi_{d,q}$(SG)	
$\lambda_{27,28}$	-2003.38	±593.27	2089.38	0.96	4.99E-04	$i_{loadD,Q}$	3
$\lambda_{29,30}$	-2634.59	±9444.63	9805.21	0.27	3.80E-04	$v_{cd,q}$	
$\lambda_{31,32}$	-2899.39	±1.11E+04	1.15E+04	0.25	3.45E-04		
$\lambda_{33,34}$	-3724.89	±1978.91	4217.93	0.88	2.68E-04	$i_{fd,q}$, $i_{line,13}$, $i_{line,23}$	
$\lambda_{35,36}$	-3848.26	±8921.38	9715.97	0.40	2.60E-04	$i_{fd,q}$, $v_{cd,q}$	
$\lambda_{37,38}$	-3882.62	±9088.95	9883.51	0.39	2.58E-04		
λ_{39}	-8.96E+06	0	8.96E+06	1	1.12E-07	φ_d, $i_{lineD,03}$	Not shown.
λ_{40}	-9.00E+06	0	9.00E+06	1	1.11E-07	φ_q, $i_{lineQ,03}$	
λ_{41}	-3.96E+07	0	3.96E+07	1	2.53E-08	$i_{line,13}$, $i_{line,23}$	
λ_{42}	-3.96E+07	0	3.96E+07	1	2.52E-08		

$$C_r = \begin{bmatrix} 505.3 & 111.9 & -201.0 \\ -113.5 & 528.7 & 1.103e3 \end{bmatrix}$$

$$D_r = \begin{bmatrix} 760.0 & -36.65 \\ -508.5 & 648.1 \end{bmatrix}$$

Reduced model derived from SP method:

$$A_s = \begin{bmatrix} -4.992 & -12.04 & -0.1842 & 27.08 \\ -0.0026 & -5.996 & 0.0146 & 0.0123 \\ 7.674 & -3.151 & -11.68 & 1.829e3 \\ -0.0012 & -0.6993 & 0.0118 & -4.759 \end{bmatrix}$$

$$B_s = \begin{bmatrix} 3.818 & -0.6065 \\ -0.3425 & 0.0083 \\ 71.81 & 11.16 \\ 1.051 & -0.0026 \end{bmatrix}$$

$$C_s = \begin{bmatrix} -57.72 & 8.875e4 & 151.6 & -1.535e5 \\ -2.332 & -9.723e3 & 179.6 & 5.111e4 \end{bmatrix}$$

$$D_s = \begin{bmatrix} -6.634e3 & -376.8 \\ 585.7 & -654.8 \end{bmatrix}$$

Reduced transfer function from $\Delta\omega_g(s)$ to $\Delta P_{oV}(s)$ derived from PCPA:

$$G_{r1}(s) = \frac{1.003e7s^2 - 1.890e8s - 5.220e9}{s^3 + 589.3s^2 + 2.447e4s + 1.089e5}$$

Reduced transfer function from $\Delta U_g(s)$ to $\Delta Q_{oV}(s)$ derived from PCPA:

$$G_{r2} = \frac{7.243s^3 - 6.459e5s^2 - 1.358e7s - 5.590e7}{s^3 + 589.3s^2 + 2.447e4s + 1.089e5}$$

Equivalent parameters derived from EqSG method: $J^{eq} = 1.012$, $D_p^{eq} = 149.9$, $K^{eq} = 0.0109$, $D_q^{eq} = 915.6$, $Z = 1.237$, $\alpha = 1.275$ and $r_x = 0.3115$.

REFERENCES

[1] U. Tamrakar, D. Shrestha, M. Maharjan, B. Bhattarai, T. Hansen, and R. Tonkoski, "Virtual inertia: Current trends and future directions," *Appl. Sci.*, vol. 7, no. 7, p. 654, Jun. 2017.

[2] Q.-C. Zhong, "Power-electronics-enabled autonomous power systems: Architecture and technical routes," *IEEE Trans. Ind. Electron.*, vol. 64, no. 7, pp. 5907–5918, Jul. 2017.

[3] B. Kroposki, B. Johnson, Y. Zhang, V. Gevorgian, P. Denholm, B.-M. Hodge, and B. Hannegan, "Achieving a 100% renewable grid: Operating electric power systems with extremely high levels of variable renewable energy," *IEEE Power Energy Mag.*, vol. 15, no. 2, pp. 61–73, Mar. 2017.

[4] H.-P. Beck and R. Hesse, "Virtual synchronous machine," in *Proc. 9th Int. Conf. Electr. Power Qual. Utilisation*, Barcelona, Spain, Oct. 2007, pp. 1–6.

[5] S. D'Arco, J. A. Suul, and O. B. Fosso, "A virtual synchronous machine implementation for distributed control of power converters in SmartGrids," *Electr. Power Syst. Res.*, vol. 122, pp. 180–197, May 2015.

[6] J. Liu, Y. Miura, H. Bevrani, and T. Ise, "Enhanced virtual synchronous generator control for parallel inverters in microgrids," *IEEE Trans. Smart Grid*, vol. 8, no. 5, pp. 2268–2277, Sep. 2017.

[7] H. Wu, X. Ruan, D. Yang, X. Chen, W. Zhao, Z. Lv, and Q.-C. Zhong, "Small-signal modeling and parameters design for virtual synchronous generators," *IEEE Trans. Ind. Electron.*, vol. 63, no. 7, pp. 4292–4303, Jul. 2016.
[8] Q.-C. Zhong and G. Weiss, "Synchronverters: Inverters that mimic synchronous generators," *IEEE Trans. Ind. Electron.*, vol. 58, no. 4, pp. 1259–1267, Apr. 2011.
[9] J. A. Suul, S. D'Arco, and G. Guidi, "Virtual synchronous machine-based control of a single-phase bi-directional battery charger for providing vehicle-to-grid services," *IEEE Trans. Ind. Appl.*, vol. 52, no. 4, pp. 3234–3244, Jul. 2016.
[10] S. D'Arco and J. A. Suul, "Equivalence of virtual synchronous machines and frequency-droops for converter-based MicroGrids," *IEEE Trans. Smart Grid*, vol. 5, no. 1, pp. 394–395, Jan. 2014.
[11] J. Liu, Y. Miura, and T. Ise, "Comparison of dynamic characteristics between virtual synchronous generator and droop control in inverter-based distributed generators," *IEEE Trans. Power Electron.*, vol. 31, no. 5, pp. 3600–3611, May 2016.
[12] Y. Hirase, K. Sugimoto, K. Sakimoto, and T. Ise, "Analysis of resonance in microgrids and effects of system frequency stabilization using a virtual synchronous generator," *IEEE J. Emerg. Sel. Topics Power Electron.*, vol. 4, no. 4, pp. 1287–1298, Dec. 2016.
[13] N. Pogaku, M. Prodanovic, and T. C. Green, "Modeling, analysis and testing of autonomous operation of an inverter-based microgrid," *IEEE Trans. Power Electron.*, vol. 22, no. 2, pp. 613–625, Mar. 2007.
[14] X. Meng, Q. Wang, N. Zhou, S. Xiao, and Y. Chi, "Multi-time scale model order reduction and stability consistency certification of inverter-interfaced DG system in AC microgrid," *Energies*, vol. 11, no. 1, p. 254, Jan. 2018.
[15] L. Fortuna, G. Nunnari, and A. Gallo, *Model Order Reduction Techniques with Applications in Electrical Engineering*. London, U.K.: Springer, 1992, pp. 11–15.
[16] V. Mariani, F. Vasca, J. C. Vásquez, and J. M. Guerrero, "Model order reductions for stability analysis of islanded microgrids with droop control," *IEEE Trans. Ind. Electron.*, vol. 62, no. 7, pp. 4344–4354, Jul. 2015.
[17] M. Rasheduzzaman, J. A. Mueller, and J. W. Kimball, "Reduced-order small-signal model of microgrid systems," *IEEE Trans. Sustain. Energy*, vol. 6, no. 4, pp. 1292–1305, Oct. 2015.
[18] L. Luo and S. V. Dhople, "Spatiotemporal model reduction of inverter-based islanded microgrids," *IEEE Trans. Energy Convers.*, vol. 29, no. 4, pp. 823–832, Dec. 2014.
[19] P. Vorobev, P.-H. Huang, M. Al Hosani, J. L. Kirtley, and K. Turitsyn, "High-fidelity model order reduction for microgrids stability assessment," *IEEE Trans. Power Syst.*, vol. 33, no. 1, pp. 874–887, Jan. 2018.
[20] F. O. Resende and J. A. P. Lopes, "Development of dynamic equivalents for microgrids using system identification theory," in *Proc. IEEE Lausanne Power Tech*, Lausanne, Switzerland, Jul. 2007, pp. 1033–1038.
[21] P. N. Papadopoulos, T. A. Papadopoulos, A. J. Roscoe, G. M. Burt, G. K. Papagiannis, and P. Crolla, "Black-box dynamic equivalent model for microgrids using measurement data," *IET Gener., Transmiss. Distribution*, vol. 8, no. 5, pp. 851–861, May 2014.
[22] P. N. Papadopoulos, G. K. Papagiannis, A. J. Roscoe, P. Crolla, T. A. Papadopoulos, and G. M. Burt, "Measurement-based analysis of the dynamic performance of microgrids using system identification techniques," *IET Gener., Transmiss. Distrib.*, vol. 9, no. 1, pp. 90–103, Jan. 2015.
[23] B. Zaker, G. B. Gharehpetian, and M. Karrari, "A novel measurement-based dynamic equivalent model of grid-connected microgrids," *IEEE Trans. Ind. Informat.*, vol. 15, no. 4, pp. 2032–2043, Apr. 2019.
[24] M. Rasheduzzaman, J. A. Mueller, and J. W. Kimball, "An accurate small-signal model of inverter-dominated islanded microgrids using *dq* reference frame," *IEEE J. Emerg. Sel. Topics Power Electron.*, vol. 2, no. 4, pp. 1070–1080, Dec. 2014.
[25] O. Mo, S. D'Arco, and J. A. Suul, "Evaluation of virtual synchronous machines with dynamic or quasi-stationary machine models," *IEEE Trans. Ind. Electron.*, vol. 64, no. 7, pp. 5952–5962, Jul. 2017.
[26] P. Krause, O. Wasynczuk, S. D. Sudhoff, and S. Pekarek, *Analysis of Electric Machinery and Drive Systems*. Hoboken, NJ, USA: Wiley, 2013, pp. 143–156.
[27] J. He, Y. W. Li, J. M. Guerrero, F. Blaabjerg, and J. C. Vasquez, "An islanding microgrid power sharing approach using enhanced virtual impedance control scheme," *IEEE Trans. Power Electron.*, vol. 28, no. 11, pp. 5272–5282, Nov. 2013.
[28] B. Moore, "Principal component analysis in linear systems: Controllability, observability, and model reduction," *IEEE Trans. Autom. Control*, vol. AC-26, no. 1, pp. 17–32, Feb. 1981.
[29] A. Laub, M. Heath, C. Paige, and R. Ward, "Computation of system balancing transformations and other applications of simultaneous diagonalization algorithms," *IEEE Trans. Autom. Control*, vol. 32, no. 2, pp. 115–122, Feb. 1987.
[30] P. V. Kokotovic, R. E. O'Malley, and P. Sannuti, "Singular perturbations and order reduction in control theory—An overview," *Automatica*, vol. 12, no. 2, pp. 123–132, Mar. 1976.
[31] R. Komarasamy, N. Albhonso, and G. Gurusamy, "Order reduction of linear systems with an improved pole clustering," *J. Vibrat. Control*, vol. 18, no. 12, pp. 1876–1885, Oct. 2012.
[32] B.-W. Wan, "Linear model reduction using mihailov criterion and Padé approximation technique," *Int. J. Control*, vol. 33, no. 6, pp. 1073–1089, Jun. 1981.
[33] J. Pal, "Improved Pade approximants using stability equation method," *Electron. Lett.*, vol. 19, no. 11, pp. 426–427, May 1983.
[34] A. K. Choudhary and S. K. Nagar, "Order reduction techniques via Routh approximation: A critical survey," *IETE J. Res.*, vol. 65, no. 3, pp. 365–379, May 2019.
[35] S. Al-Dabooni and D. Wunsch, "Model order reduction based on agglomerative hierarchical clustering," *IEEE Trans. Neural Netw. Learn. Syst.*, vol. 30, no. 6, pp. 1881–1895, Jun. 2019.

WENQIANG HU (Student Member, IEEE) received the B.Eng. degree in electrical engineering and its automation from the China University of Petroleum (East China), Qingdao, China, in 2015. He is currently pursuing the Ph.D. degree in electrical engineering with Southeast University, Nanjing, China. He was a Visiting Ph.D. Student with the University of Alberta, Edmonton, AB, Canada. His research interests include power electronics control, distributed generation, and microgrid.

ZAIJUN WU (Member, IEEE) received the B.Eng. degree in power system and its automation from the Hefei University of Technology, Hefei, China, in 1996, and the Ph.D. degree in electrical engineering from Southeast University, Nanjing, China, in 2004. From 2012 to 2013, he was a Visiting Scholar with The Ohio State University, Columbus, OH, USA. He is currently a Professor in electrical engineering with the School of Electrical Engineering, Southeast University. He is the author or coauthor of more than 100 refereed journal articles. His research interests include microgrid, active distribution networks, and power quality. He is a reviewer of several journals.

VENKATA DINAVAHI (Fellow, IEEE) received the B.Eng. degree in electrical engineering from the Visveswaraya National Institute of Technology (VNIT), Nagpur, India, in 1993, the M.Tech. degree in electrical engineering from the Indian Institute of Technology (IIT) Kanpur, India, in 1996, and the Ph.D. degree in electrical and computer engineering from the University of Toronto, Toronto, ON, Canada, in 2000. He is currently a Professor with the Department of Electrical and Computer Engineering, University of Alberta, Edmonton, AB, Canada. His research interests include real-time simulation of power systems and power electronic systems, electromagnetic transients, device-level modeling, large-scale systems, and parallel and distributed computing.